***New Phytologist* Supporting Information**

Article title: Evaluating the kinetic basis of plant growth from organs to ecosystems
Authors: Sean T. Michaletz (michaletz@email.arizona.edu)
Article acceptance date: 18 December 2017

The following Supporting Information is available for this article:

Fig. S1 A typical temperature response curve for a biological rate.

Fig. S2 Modified Arrhenius plots of Sharpe-Schoolfield model fits (with E_h as a free parameter) to photosynthesis temperature response data.

Fig. S3 Modified Arrhenius plots of Sharpe-Schoolfield model fits (with E_h as a fixed parameter) to photosynthesis temperature response data.

Fig. S4 Tree growth rates across a broad air temperature gradient.

Fig. S5 Distributions of intraspecific optimal temperatures for photosynthesis, estimated from Eqn (2) with E_h as a free parameter.

Fig. S6 Distributions of intraspecific optimal temperatures for photosynthesis, estimated from Eqn (2) with E_h as a fixed parameter.

Table S1 List of taxa, number of curves per taxon, and primary sources for photosynthesis temperature response data used in analyses.

Table S2 List of growth variables, temperature variables, sample sizes, and primary sources for growth analyses.

Methods S1 Description of data and methods used for analyses.

Notes S1 R code for fitting the Sharpe-Schoolfield model (TPCfitting_stm.R).

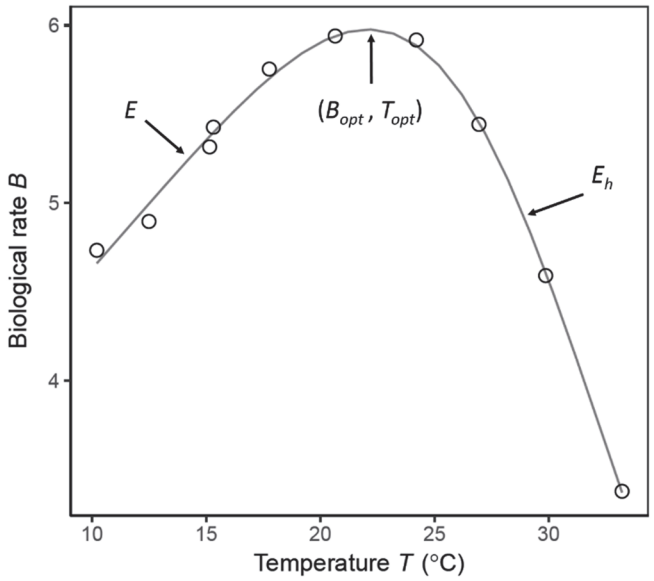

Fig. S1 A typical temperature response curve for a biological rate. In general, biological rates B increase with temperature T to a maximum value B_{opt} at an optimal temperature T_{opt}, and then decrease with temperature above this optimum. The effective activation energy E and the enzyme inactivation parameter E_h (both nonlinear in this space) influence the increasing and decreasing portions of the curve, respectively, as formalized in Eqn (2). Data points are net photosynthesis (μmol m^{-2} s^{-1}) of *Juniperus monosperma* (Michaletz *et al.*, 2016b), and solid line is a fitted Sharpe-Schoolfield model (Eqn (2)).

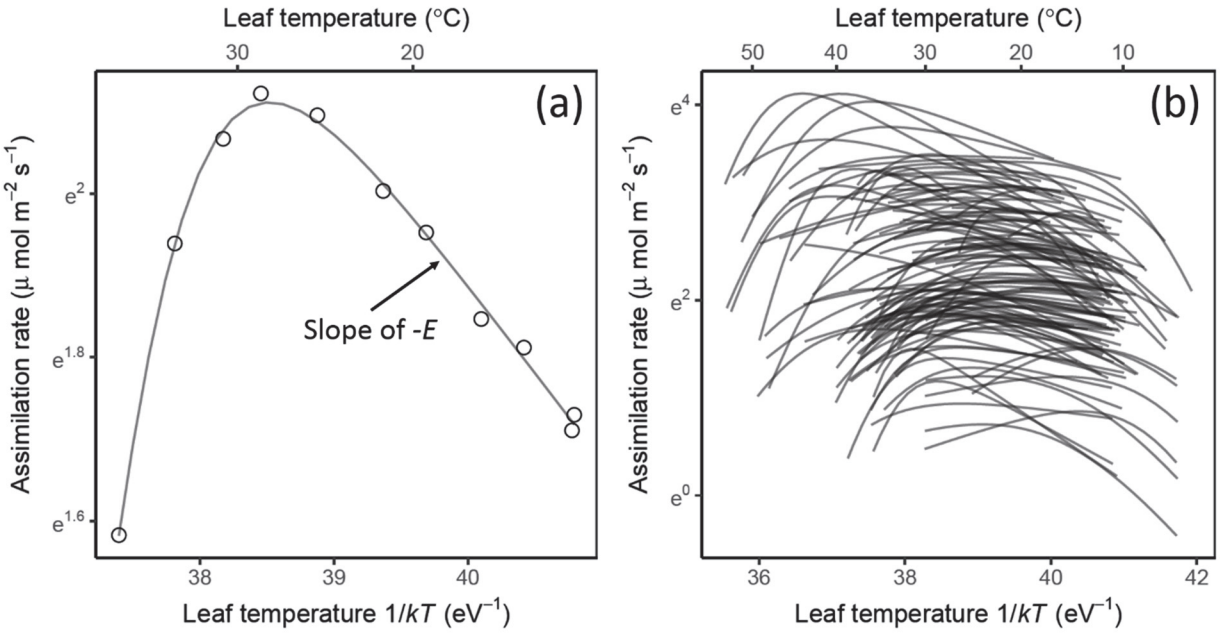

Fig. S2 Modified Arrhenius plots of Sharpe-Schoolfield model (Eqn (2)) fits (with E_h as a free parameter) to photosynthesis temperature response data for (a) an individual *Juniperus monosperma* leaf cluster (E = 0.22 eV, quasi r^2 = 0.996) and (b) 119 leaves from 32 species (E = 0.03 to 3.06 eV, quasi r^2 = 0.672 to 1.000). Relationships are presented as modified Arrhenius plots that linearize assimilation rates relative to leaf temperature 1/kT, yielding a linear slope of -E on the decreasing portion of the curve. Data used in analyses are described in Table S1.

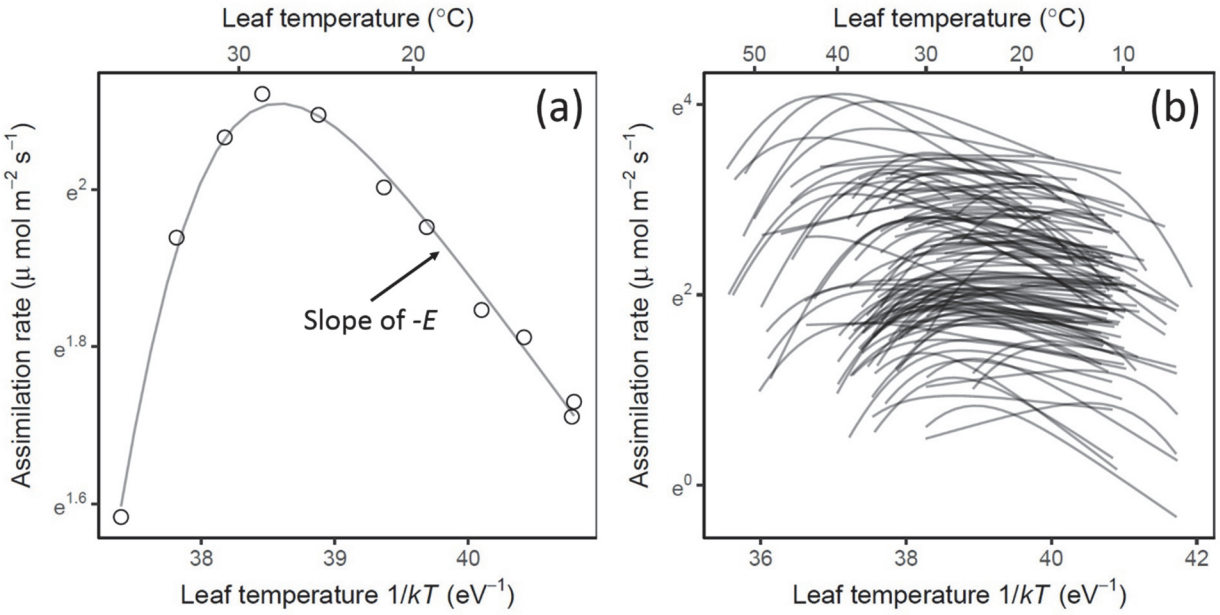

Fig. S3 Modified Arrhenius plots of Sharpe-Schoolfield model (Eqn (2)) fits (with E_h as a fixed parameter) to photosynthesis temperature response data for (a) an individual *Juniperus monosperma* leaf cluster (E = 0.24 eV, quasi r^2 = 0.993) and (b) 119 leaves from 32 species (E = 1.98 x 10^{-8} to 2.07 eV, quasi r^2 = 0.146 to 0.999). Relationships are presented as modified Arrhenius plots that linearize assimilation rates relative to leaf temperature 1/kT, yielding a linear slope of -E on the decreasing portion of the curve. Data used in analyses are described in Table S1.

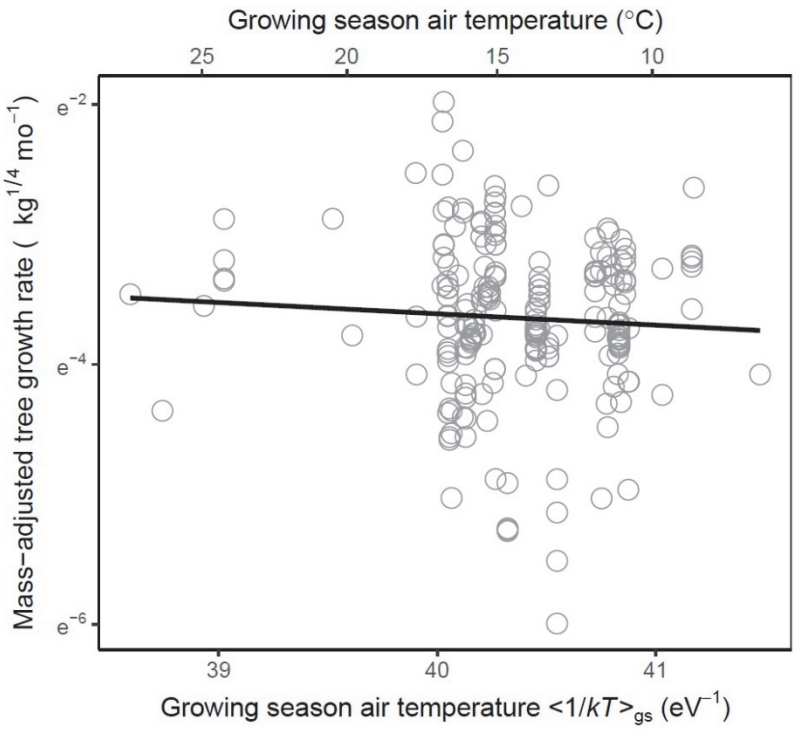

Fig. S4 Tree growth rates across a broad air temperature gradient (*N* = 210). Data from Fig. 2b replotted with within-site measurements treated as independent samples rather than site means. The same general results are observed here and in Fig. 2b. Tree growth rate was invariant with air temperature (*P* = 0.373, r^2 = 0.004). The fitted *E* = 0.09 has 95% CI = -0.11 to 0.28 that exclude hypothesized values of 0.32 eV (Allen *et al.*, 2005) and 0.65 eV for respiration (Gillooly *et al.*, 2001). This is a modified Arrhenius plot that linearizes the relationship between growth and temperature to yield a slope *–E* that is equal in magnitude but opposite in direction to the activation energy *E* (Eqns (1) and (S1)). Temperature is quantified as $1/kT$ (eV^{-1}), where *k* (8.617×10^{-5} eV K^{-1}) is Boltzmann's constant and *T* (K) is air temperature. Tree growth rates are expressed as mass-adjusted rates, $BM^{-3/4} = B_1 e^{-E/kT}$. This relationship is obtained via rearrangement of $B = B_1 M^{3/4} e^{-E/kT}$, which is in turn obtained by unpacking the normalization constant B_0 in Eqn (1) to reveal the influence of biomass *M*, where B_1 is a biomass-independent normalization constant. Data from Enquist *et al*. (2007).

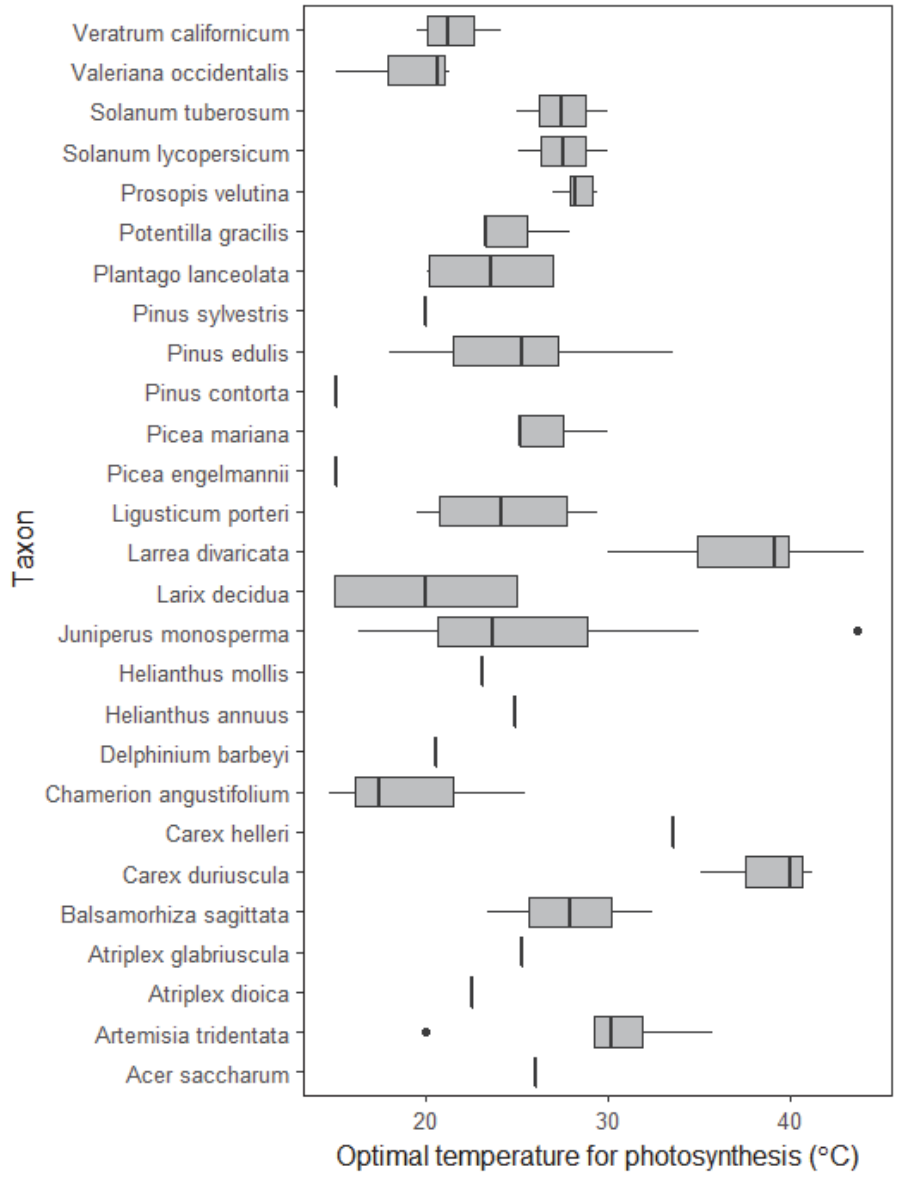

Fig. S5 Distributions of intraspecific optimal temperatures for photosynthesis, estimated from Eqn (2) with E_h as a free parameter. Optimal temperatures for photosynthesis vary substantially within and among species, reflecting acclimation and local adaptation of photosynthetic traits to site-averaged leaf operating temperatures. The mean optimal temperature across all samples is 25.66 ˚C. Thick black lines correspond to medians, lower and upper hinges correspond to first and third quartiles, respectively, lower and upper whiskers correspond to smallest and largest values that do not exceed 1.5 times the interquartile range of the hinges, respectively, and points correspond to outliers beyond the end of the whiskers.

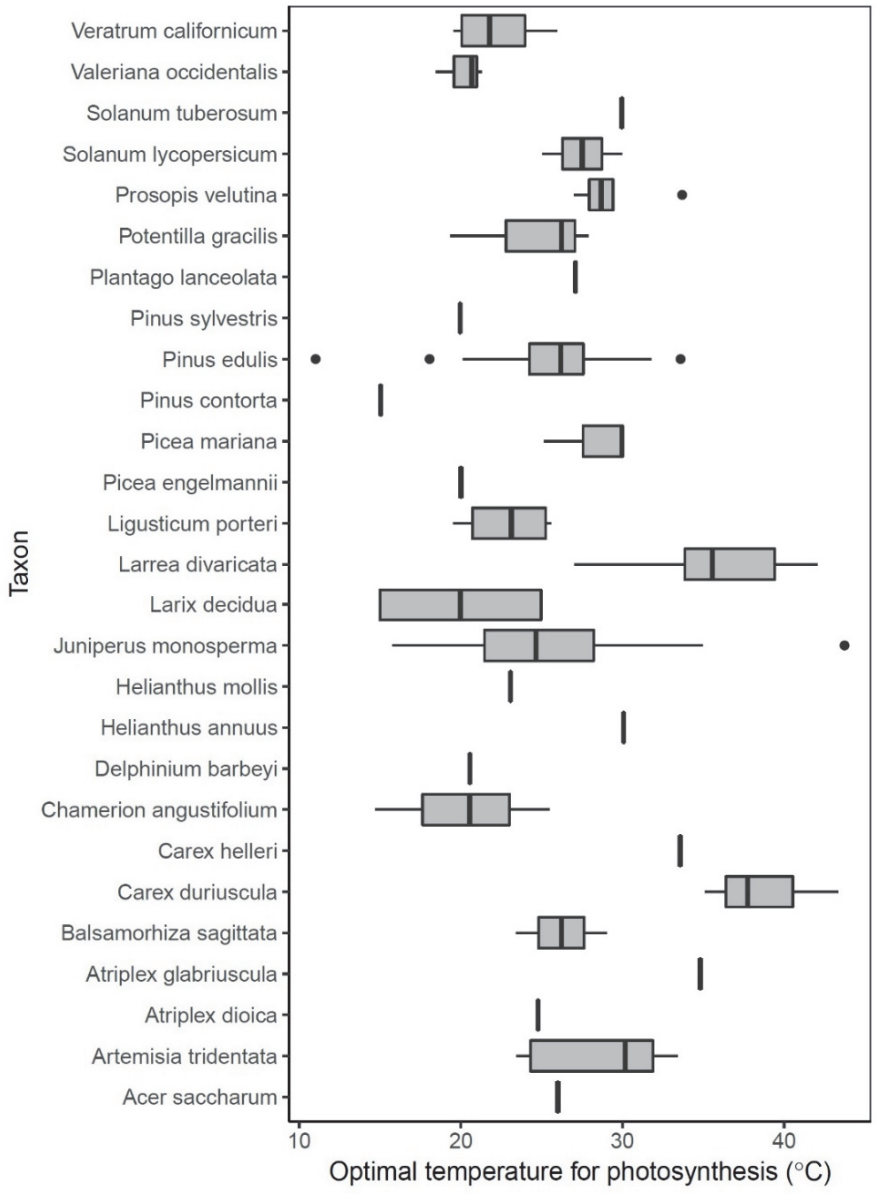

Fig. S6 Distributions of intraspecific optimal temperatures for photosynthesis, estimated from Eqn (2) with E_h as a fixed parameter. Optimal temperatures for photosynthesis vary substantially within and among species, reflecting acclimation and local adaptation of photosynthetic traits to site-averaged leaf operating temperatures. The mean optimal temperature across all samples is 26.21 ˚C. Thick black lines correspond to medians, lower and upper hinges correspond to first and third quartiles, respectively, lower and upper whiskers correspond to smallest and largest values that do not exceed 1.5 times the interquartile range of the hinges, respectively, and points correspond to outliers beyond the end of the whiskers.

Table S1 List of taxa, number of curves per taxon, and primary sources for photosynthesis temperature response data used in analyses

Taxon	Number of curves	Primary source
Acer saccharum	1	Gunderson *et al*. (2000)
Artemisia tridentata	5	Michaletz *et al*. (2016b)
Atriplex dioica	1	Sage *et al*. (2011)
Atriplex glabriuscula	1	Osmond *et al*. (1980)
Balsamorhiza sagittata	2	Michaletz *et al*. (2015)
Carex duriuscula	3	Monson *et al*. (1983)
Carex helleri	1	Sage *et al*. (2011)
Chamerion angustifolium	3	Michaletz *et al*. (2016b)
Delphinium barbeyi	1	Michaletz *et al*. (2016b)
Helianthus annuus	1	Paul *et al*. (1990)
Helianthus mollis	1	Zhou *et al*. (2007)
Juniperus monosperma	31	Michaletz *et al*. (2016b)
Larix decidua	4	Tranquillini *et al*. (1986)
Larrea divaricata	7	Mooney *et al*. (1978)
Ligusticum porteri	4	Michaletz *et al*. (2016b)
Picea engelmannii	1	Huxman *et al*. (2003)
Picea mariana	3	Way & Sage (2008a) (2008b)
Pinus contorta	1	Huxman *et al*. (2003)
Pinus edulis	21	Michaletz *et al*. (2016b)
Pinus sylvestris	1	Wang *et al*. (1996)
Plantago lanceolata	4	Atkin *et al*. (2006)
Potentilla gracilis	3	Michaletz *et al*. (2016b)
Prosopis velutina	6	Barron-Gafford *et al*. (2012)
Solanum lycopersicum	2	Yamori *et al*. (2010)
Solanum tuberosum	2	Yamori *et al*. (2010)
Valeriana occidentalis	3	Michaletz *et al*. (2016b)
Veratrum californicum	6	Michaletz *et al*. (2016b)

Table S2 List of growth variables, temperature variables, sample sizes, and primary sources for growth analyses

Level of organization	Growth variable	Temperature variable	Sample size	Primary source
Organ	Root meristem cell doubling rate (h^{-1})	Cell temperature (˚C)	60	Körner (2003a)
Individual	Mass-adjusted individual tree growth rate ($kg^{1/4}$ mo^{-1})	Growing season air temperature (˚C)	210	Enquist *et al*. (2007)
Ecosystem	Adjusted net primary production (kg m^{-2} mo^{-1})	Growing season air temperature (˚C)	138	Michaletz *et al*. (2014; 2016a)

Methods S1 Description of data and methods used for analyses.

Photosynthesis temperature response data and Sharpe-Schoolfield fitting procedures

Photosynthesis temperature response curves were obtained from Michaletz *et al*. (2016b). All curves were unimodal (e.g. see Fig. S1) and comprise data measured in Colorado and New Mexico, as well as compiled from the literature. Further details on measurement methodologies are available in the primary sources. A total of 184 curves from 32 species were available. Taxa, number of curves per taxa, and primary sources are summarized in Table S1. These temperature response data were used to estimate activation energies E for net photosynthesis.

Various approaches can be used to estimate activation energies E from unimodal temperature response data. For example, the Boltzmann-Arrhenius model (Eqn (1)) can be fit separately to the increasing and decreasing portions of the curve, yielding separate estimates of E for each portion (Knies & Kingsolver, 2010; Dell *et al.*, 2011). However, such estimates can be strongly biased by the temperature ranges used to define the increasing and decreasing portions of the curve (Knies & Kingsolver, 2010; Pawar *et al.*, 2016). Thus, in this paper, activation energies E for net photosynthesis were estimated using Sharpe-Schoolfield model fits (Sharpe & DeMichele, 1977; Schoolfield *et al.*, 1981). This approach can help reduce bias and variation in estimates of E as compared with the Boltzmann-Arrhenius approach described above (Pawar *et al.*, 2016). Following recent methodology, Eqn (2) was fit to curves for which photosynthesis was measured at a minimum of five temperatures spanning a range of at least 5 ˚C (Dell *et al.*, 2011; Pawar *et al.*, 2016), yielding a total of 119 fitted curves from 27 species (Figs S2, S3). Fitting was accomplished using Levenberg-Marquardt nonlinear regression with Gaussian random starting values, followed by AICc model selection from 100 fits for each curve. Model fitting was conducted in the statistical software R using a modified version of code provided by Tony Dell, Samraat Pawar, and Sofia Sal (see Notes S1).

Eqn (2) has been suggested to be over-parameterized for some photosynthesis datasets that are relatively limited in the number of observations or range of temperatures (Harley *et al.*, 1992; Dreyer *et al.*, 2001; Medlyn *et al.*, 2002). Thus, I also conducted a second set of Sharpe-Schoolfield model fits using a fixed value of E_h = 200 kJ mol^{-1} = 2.073 eV. This value has been used in many previous studies (Farquhar *et al.*, 1980; Medlyn *et al.*, 2002; Slot & Winter, 2017; Stinziano *et al.*, In press), and originates from data for J_{max} in *Hordeum vulgare* (Nolan & Smillie, 1976). However, estimates of E_h for J_{max} are available for other taxa (Dreyer *et al.*, 2001; Leuning, 2002; Warren & Dreyer, 2006; Galmés *et al.*, 2015), and these estimates show that of E_h varies more than 8-fold across taxa (Dreyer *et al.*, 2001). It is thus unclear how appropriate it is to apply a single fixed value of E_h for J_{max} from a single species to net photosynthesis data for diverse taxa (as in Table S1). Additionally, the data used here were all unimodal with a relatively large number of observations and range of temperatures (e.g. Figs S1-S3). It may be for these reasons that the Sharpe-Schoolfield model provided vastly better fits to data (Table S1) when E_h was taken as a free parameter (quasi r^2 = 0.672 to 1.000) rather than a fixed parameter (quasi r^2 = 0.146 to 0.999).

Perhaps a better alternative to a fixed E_h is to use a free E_h and reject fitted curves based on standard errors of estimates for each parameter (cf. Pawar *et al.*, 2016). Nonetheless, evaluation of Sharpe-Schoolfield fitting procedures is beyond the scope of this paper, and the above two approaches are presented in order to highlight the sensitivity of E to Sharpe-Schoolfield fitting procedures.

Plant growth data and Boltzmann-Arrhenius fitting procedures

Plant growth data were compiled and analyzed for three levels of biological organization: organs, individuals, and ecosystems. Root organ growth data (Fig. 2a) were obtained from Figure 3 of Körner (2003b), which is a compilation of data from approximately 50 primary sources. Data are division rates of root meristem cells. For land plants, root meristem cells provide one of the most accurate and resolved measures of *in situ* growth rates, for three reasons. First, rates of cell division are tightly coupled to rates of cell differentiation, when most

biomass growth occurs (Körner, 2003a; Körner, 2012). Second, root operative temperatures are in thermal equilibrium with soil, so they are relatively straightforward to control and quantify (unlike aboveground organs; Michaletz *et al.*, 2015; Michaletz *et al.*, 2016b). Third, cell size is essentially constant, which eliminates confounding effects of biomass. Data were extracted from Figure 3 using the software DataThief III v1.7. Data were given as cell doubling times (h), which were calculated as the statistical means across all cells within a meristematic region. The inverse of cell doubling times was used to calculate the cell growth rates (h^{-1}) that were used in Fig. 2a.

Individual growth data (Fig. 2b) were obtained from Enquist et al. (2007). Data comprise mass-adjusted tree growth rates that control for variation in tree size and growing season length (mo yr^{-1}), which is needed to properly evaluate temperature effects on plant metabolic kinetics (Michaletz *et al.*, In press). Growth rates correspond to total (above- plus belowground) biomass growth. Mass-adjusted rates $BM^{-3/4}$ ($kg^{1/4}$ mo^{-1}) are given by $BM^{-3/4} = B_1 e^{-E/kT}$ (Brown & Sibly, 2012; White *et al.*, 2012), where B (kg mo^{-1}) is the seasonal growth rate (Michaletz *et al.*, In press), M (kg) is the total tree biomass, and the 3/4 scaling exponent is based on extensive empirical and theoretical support (Brown & Sibly, 2012). Since multiple growth rate data were available for some sites in this dataset, they were taken as the mean ± 1 standard error in Fig. 2b (although the same general results were obtained when these were treated as independent samples; Fig. S4). Air temperature data are based on monthly average air temperatures during the growing season (including day and night). Growing season air temperature is the monthly average air temperature during the growing season months (including day and night). Data were calculated from site latitude and longitude and a gridded global climate dataset (New *et al.*, 2002). This data set interpolates weather station data, so these temperatures correspond to weather station standards and not plant operative temperatures. Growing season months were estimated from air temperature, precipitation, and potential evapotranspiration data as described in Kerkhoff *et al*. (2005).

Ecosystem production data (Fig. 2c) were obtained from Michaletz *et al*. (2016a), which is a subset of data compiled by Michaletz *et al*. (2014). Data are monthly net primary production (NPP; kg m^{-2} mo^{-1}) rates calculated over the growing season (mo yr^{-1}). Fig. 2c is a partial regression plot that shows the correct relationship (slope and variance) between net primary production and temperature while controlling for the influence of biomass, age, and precipitation. In this analysis, samples from the same latitude and longitude that share temperature and precipitation data all have unique data for age and/or stand biomass, and are thus treated as independent samples. Air temperature data are based on monthly average air temperatures during the growing season (including day and night). Growing season air temperature is the monthly average air temperature during the growing season months (including day and night). Data were calculated from site latitude and longitude and a gridded global climate dataset (New *et al.*, 2002). This data set interpolates weather station data, so these temperatures correspond to standard weather station measurements and not plant operative temperatures. Growing season months were estimated from air temperature, precipitation, and potential evapotranspiration data as described in Michaletz *et al*. (2014).

Since organ, individual, and ecosystem-level growth data correspond to temperatures below those optimal for plant metabolism (Figs S5, S6; Dell *et al.*, 2011; Slot & Winter, 2017), activation energies E were estimated using Boltzmann-Arrhenius model fits. Specifically, Eqn (1) was $\log_e$-transformed to give the growth rate B as

$$\ln\left(B\right) = \ln\left(B_0\right) - E\frac{1}{kT} \tag{S1}$$

where B_0 is a normalization constant that implicitly includes effects of other variables not considered here, k is the Boltzmann constant (8.617 x 10^{-5} eV K^{-1}), and E (eV) is an effective activation energy that characterizes the temperature-dependence of the rate under consideration. Note that here, the units of B and B_0 will vary depending on the growth rate under consideration (h^{-1} for cells, $kg^{1/4}$ mo^{-1} for individuals, and kg m^{-2} mo^{-1} for ecosystems). These $\log_e$-scaled growth data were then regressed over temperature $1/kT$, to produce modified Arrhenius plots (Fig. 2) with a slope $-E$ that is equal in magnitude but opposite in direction to the activation energy E.

References

Allen AP, Gillooly JF, Brown JH. 2005. Linking the global carbon cycle to individual metabolism. *Functional Ecology* **19**: 202-213.

Atkin OK, Scheurwater I, Pons TL. 2006. High thermal acclimation potential of both photosynthesis and respiration in two lowland *Plantago* species in contrast to an alpine congeneric. *Global Change Biology* **12**: 500-515.

Barron-Gafford GA, Scott RL, Jenerette GD, Hamerlynck EP, Huxman TE. 2012. Temperature and precipitation controls over leaf- and ecosystem-level CO_2 flux along a woody plant encroachment gradient. *Global Change Biology* **18**: 1389-1400.

Brown JH, Sibly RM 2012. The metabolic theory of ecology and its central equation. In: Sibly RM, Brown JH eds. *Metabolic ecology: A scaling approach*. New York: John Wiley & Sons, Ltd., 21-33.

Dell AI, Pawar S, Savage VM. 2011. Systematic variation in the temperature dependence of physiological and ecological traits. *Proceedings of the National Academy of Sciences* **108**: 10591-10596.

Dreyer E, Le Roux X, Montpied P, Daudet FA, Masson F. 2001. Temperature response of leaf photosynthetic capacity in seedlings from seven temperate tree species. *Tree Physiology* **21**: 223-232.

Enquist BJ, Kerkhoff AJ, Huxman TE, Economo EP. 2007. Adaptive differences in plant physiology and ecosystem paradoxes: Insights from metabolic scaling theory. *Global Change Biology* **13**: 591-609.

Farquhar GD, von Caemmerer S, Berry JA. 1980. A biochemical model of photosynthetic CO_2 assimilation in leaves of C_3 species. *Planta* **149**: 78-90.

Galmés J, Kapralov MV, Copolovici LO, Hermida-Carrera C, Niinemets Ü. 2015. Temperature responses of the Rubisco maximum carboxylase activity across domains of life: Phylogenetic signals, trade-offs, and importance for carbon gain. *Photosynthesis Research* **123**: 183-201.

Gillooly JF, Brown JH, West GB, Savage VM, Charnov EL. 2001. Effects of size and temperature on metabolic rate. *Science* **293**: 2248-2251.

Gunderson CA, Norby RJ, Wullschleger SD. 2000. Acclimation of photosynthesis and respiration to simulated climatic warming in northern and southern populations of *Acer saccharum*: Laboratory and field evidence. *Tree Physiology* **20**: 87-96.

Harley PC, Thomas RB, Reynolds JF, Strain BR. 1992. Modelling photosynthesis of cotton grown in elevated CO2. *Plant, Cell & Environment* **15**: 271-282.

Huxman TE, Turnipseed AA, Sparks JP, Harley PC, Monson RK. 2003. Temperature as a control over ecosystem CO_2 fluxes in a high-elevation, subalpine forest. *Oecologia* **134**: 537-546.

Kerkhoff AJ, Enquist BJ, Elser JJ, Fagan WF. 2005. Plant allometry, stoichiometry and the temperature-dependence of primary productivity. *Global Ecology and Biogeography* **14**: 585-598.

Knies Jennifer L, Kingsolver JG. 2010. Erroneous arrhenius: Modified arrhenius model best explains the temperature dependence of ectotherm fitness. *The American Naturalist* **176**: 227-233.

Körner C. 2003a. *Alpine plant life: Functional plant ecology of high mountain ecosystems. Second edition.* New York: Springer.

Körner C. 2003b. Carbon limitation in trees. *Journal of Ecology* **91**: 4-17.

Körner C. 2012. *Alpine treelines: Functional ecology of the global high elevation tree limits*. Basel, Switzerland: Springer Science & Business Media.

Leuning R. 2002. Temperature dependence of two parameters in a photosynthesis model. *Plant, Cell & Environment* **25**: 1205-1210.

Medlyn BE, Dreyer E, Ellsworth D, Forstreuter M, Harley PC, Kirschbaum MUF, Le Roux X, Montpied P, Strassemeyer J, Walcroft A, et al. 2002. Temperature response of parameters of a biochemically based model of photosynthesis. II. A review of experimental data. *Plant, Cell & Environment* **25**: 1167-1179.

Michaletz ST, Cheng D, Kerkhoff AJ, Enquist BJ. 2014. Convergence of terrestrial plant production across global climate gradients. *Nature* **512**: 39-43.

Michaletz ST, Cheng D, Kerkhoff AJ, Enquist BJ. 2016a. Corrigendum: Convergence of terrestrial plant production across global climate gradients. *Nature* **537**: 432-432.

Michaletz ST, Kerkhoff AJ, Enquist BJ. In press. Drivers of terrestrial plant production across broad geographic gradients. *Global Ecology and Biogeography*. DOI: 10.1111/geb.12685.

Michaletz ST, Weiser MD, McDowell NG, Zhou J, Kaspari M, Helliker BR, Enquist BJ. 2016b. The energetic and carbon economic origins of leaf thermoregulation. *Nature Plants* **2**: 16129.

Michaletz ST, Weiser MD, Zhou J, Kaspari M, Helliker BR, Enquist BJ. 2015. Plant thermoregulation: Energetics, trait-environment interactions, and carbon economics. *Trends in Ecology & Evolution* **30**: 714-724.

Monson R, Littlejohn R, Jr., Williams G, III. 1983. Photosynthetic adaptation to temperature in four species from the Colorado shortgrass steppe: A physiological model for coexistence. *Oecologia* **58**: 43-51.

Mooney HA, Björkman O, Collatz GJ. 1978. Photosynthetic acclimation to temperature in the desert shrub, *Larrea divaricata*: I. Carbon dioxide exchange characteristics of intact leaves. *Plant Physiology* **61**: 406-410.

New M, Lister D, Hulme M, Makin I. 2002. A high-resolution data set of surface climate over global land areas. *Climate Research* **21**: 1-25.

Nolan WG, Smillie RM. 1976. Multi-temperature effects on hill reaction activity of barley chloroplasts. *Biochimica et Biophysica Acta (BBA) - Bioenergetics* **440**: 461-475.

Osmond CB, Bjorkman O, Anderson DJ. 1980. *Physiological processes in plant ecology: Toward a synthesis with Atriplex*. New York: Springer-Verlag.

Paul MJ, Lawlor DW, Driscoll SP. 1990. The effect of temperature on photosynthesis and carbon fluxes in sunflower and rape. *Journal of Experimental Botany* **41**: 547-555.

Pawar S, Dell AI, Savage VM, Knies JL. 2016. Real versus artificial variation in the thermal sensitivity of biological traits. *The American Naturalist* **187**: E41-E52.

Sage R, Kocacinar F, Kubien D 2011. C_4 photosynthesis and temperature. In: Raghavendra AS, Sage RF eds. *C_4 photosynthesis and related CO_2 concentrating mechanisms*: Springer Netherlands, 161-195.

Schoolfield RM, Sharpe PJH, Magnuson CE. 1981. Non-linear regression of biological temperature-dependent rate models based on absolute reaction-rate theory. *Journal of Theoretical Biology* **88**: 719-731.

Sharpe PJH, DeMichele DW. 1977. Reaction kinetics of poikilotherm development. *Journal of Theoretical Biology* **64**: 649-670.

Slot M, Winter K. 2017. In situ temperature relationships of biochemical and stomatal controls of photosynthesis in four lowland tropical tree species. *Plant, Cell & Environment* **40**: 3055-3068.

Stinziano JR, Way DA, Bauerle WL. In press. Improving models of photosynthetic thermal acclimation: Which parameters are most important and how many should be modified? *Global Change Biology*. DOI: 10.1111/gcb.13924.

Tranquillini W, Havranek WM, Ecker P. 1986. Effects of atmospheric humidity and acclimation temperature on the temperature response of photosynthesis in young *Larix decidua* Mill. *Tree Physiology* **1**: 37-45.

Wang K-Y, Kellomäki S, Laitinen K. 1996. Acclimation of photosynthetic parameters in Scots pine after three years exposure to elevated temperature and CO_2. *Agricultural and Forest Meteorology* **82**: 195-217.

Warren CR, Dreyer E. 2006. Temperature response of photosynthesis and internal conductance to CO2: Results from two independent approaches. *Journal of Experimental Botany* **57**: 3057-3067.

Way DA, Sage RF. 2008a. Elevated growth temperatures reduce the carbon gain of black spruce [*Picea mariana* (Mill.) B.S.P.]. *Global Change Biology* **14**: 624-636.

Way DA, Sage RF. 2008b. Thermal acclimation of photosynthesis in black spruce [*Picea mariana* (Mill.) B.S.P.]. *Plant, Cell & Environment* **31**: 1250-1262.

White EP, Xiao X, Isaac NJB, Sibly RM 2012. Methodological tools. In: Sibly RM, Brown JH, Kodric-Brown A eds. *Metabolic ecology: A scaling approach*. Hoboken, New Jersey: Wiley-Blackwell, 9-20.

Yamori W, Noguchi K, Hikosaka K, Terashima I. 2010. Phenotypic plasticity in photosynthetic temperature acclimation among crop species with different cold tolerances. *Plant Physiology* **152**: 388-399.

Zhou X, Liu X, Wallace LL, Luo Y. 2007. Photosynthetic and respiratory acclimation to experimental warming for four species in a tallgrass prairie ecosystem. *Journal of Integrative Plant Biology* **49**: 270-281.